© 2016. Published by The Company of Biologists Ltd | Journal of Cell Science (2016) 129, 1155-1164 doi:10.1242/jcs.180448

RESEARCH ARTICLE

A tetraspanin regulates septate junction formation in *Drosophila* midgut

Yasushi Izumi[1,2,‡], Minako Motoishi[3], Kyoko Furuse[1] and Mikio Furuse[1,2,‡]

ABSTRACT

Septate junctions (SJs) are membrane specializations that restrict the free diffusion of solutes through the paracellular pathway in invertebrate epithelia. In arthropods, two morphologically different types of septate junctions are observed; pleated (pSJs) and smooth (sSJs), which are present in ectodermally and endodermally derived epithelia, respectively. Recent identification of sSJ-specific proteins, Mesh and Ssk, in *Drosophila* indicates that the molecular compositions of sSJs and pSJs differ. A deficiency screen based on immunolocalization of Mesh identified a tetraspanin family protein, Tsp2A, as a newly discovered protein involved in sSJ formation in *Drosophila*. Tsp2A specifically localizes at sSJs in the midgut and Malpighian tubules. Compromised Tsp2A expression caused by RNAi or the CRISPR/Cas9 system was associated with defects in the ultrastructure of sSJs, changed localization of other sSJ proteins, and impaired barrier function of the midgut. In most *Tsp2A* mutant cells, Mesh failed to localize to sSJs and was distributed through the cytoplasm. Tsp2A forms a complex with Mesh and Ssk and these proteins are mutually interdependent for their localization. These observations suggest that Tsp2A cooperates with Mesh and Ssk to organize sSJs.

KEY WORDS: *Drosophila*, Midgut, Epithelial cells, Smooth septate junction, Tetraspanin

INTRODUCTION

Epithelia separate distinct fluid compartments within the bodies of metazoans. For this epithelial function, specialized intercellular junctions, designated as occluding junctions, regulate the free diffusion of solutes through the paracellular pathway. In vertebrates, tight junctions act as occluding junctions, whereas in invertebrates, septate junctions (SJs) are the functional counterparts of tight junctions (Anderson and Van Itallie, 2009; Furuse and Tsukita, 2006; Lane et al., 1994; Tepass and Hartenstein, 1994). Septate junctions form circumferential belts around the apicolateral regions of epithelial cells. In transmission electron microscopy, septate junctions are observed between the parallel plasma membranes of adjacent cells, with ladder-like septa spanning the intermembrane space (Lane et al., 1994; Tepass and Hartenstein, 1994). Septate junctions are subdivided into several morphological types that differ among different animal phyla, and several phyla possess multiple types of septate junctions that vary among different types of epithelia (Banerjee et al., 2006; Green and Bergquist, 1982; Lane et al., 1994).

[1]Division of Cerebral Structure, National Institute for Physiological Sciences, Okazaki 444-8787, Japan. [2]Department of Physiological Sciences, SOKENDAI (The Graduate University for Advanced Studies), Okazaki 444-8585, Japan. [3]Laboratory of Regeneration Biology, Graduate School of Life Science, University of Hyogo, 3-2-1 Kouto, Kamigori-cho, Ako-gun, Hyogo 678-1297, Japan).

[‡]Authors for correspondence (furuse@nips.ac.jp; yizumi@nips.ac.jp)

Received 13 September 2015; Accepted 27 January 2016

In arthropods, two types of septate junctions exist; pleated (pSJs) and smooth (sSJs) (Banerjee et al., 2006; Lane et al., 1994; Tepass and Hartenstein, 1994). pSJs are found in ectodermally derived epithelia and surface glia surrounding the nerve cord, whereas sSJs are found mainly in endodermally derived epithelia, such as the midgut and the gastric caeca (Lane et al., 1994; Tepass and Hartenstein, 1994). The outer epithelial layer of the proventriculus (OELP) and the Malpighian tubules also possess sSJs, although these epithelia are ectodermal derivatives (Lane et al., 1994; Tepass and Hartenstein, 1994). The criteria distinguishing these two types of septate junctions are the arrangement of the septa; in oblique sections of lanthanum-treated preparations, the septa of pSJs are visualized as regular undulating rows, but those in sSJs are observed as regularly spaced parallel lines (Lane et al., 1994; Lane and Swales, 1982). In freeze-fracture images, the rows of intramembrane particles in pSJs are separated from one another, whereas those in sSJs are fused into ridges (Lane et al., 1994; Lane and Swales, 1982). To date, more than 20 pSJ-related proteins, including pSJ components and regulatory proteins involved in pSJ assembly, have been identified and characterized in *Drosophila* (Banerjee et al., 2006; Byri et al., 2015; Deligiannaki et al., 2015; Hildebrandt et al., 2015; Izumi and Furuse, 2014; Tepass et al., 2001; Wu and Beitel, 2004). By contrast, few genetic and molecular analyses have been carried out on sSJs. Recently, two sSJ-specific membrane proteins, Ssk and Mesh, have been identified and characterized (Izumi and Furuse, 2014; Izumi et al., 2012; Yanagihashi et al., 2012). Ssk consists of 162 amino acids and has four membrane-spanning domains, two short extracellular loops, cytoplasmic N- and C-terminal domains, and a cytoplasmic loop (Yanagihashi et al., 2012). Mesh has a single-pass transmembrane domain and a large extracellular region containing a NIDO domain, an Ig-like E set domain, an AMOP domain, a vWD domain, and a sushi domain (Izumi et al., 2012). Mesh transcripts are predicted to be translated into three isoforms of which the longest isoform consists of 1454 amino acids. In western blot studies, Mesh is detected as a main ∼90 kDa band and a minor ∼200 kDa band (Izumi et al., 2012). Compromised expression of *Ssk* or *mesh* causes defects in the ultrastructure of sSJs and in the barrier function of the midgut against a 10-kDa fluorescent tracer (Izumi et al., 2012; Yanagihashi et al., 2012). Ssk and Mesh physically interact with each other and are mutually dependent for their sSJ localization (Izumi et al., 2012). Thus, Mesh and Ssk play crucial roles in the formation and barrier function of sSJs.

Tetraspanins are a family of integral membrane proteins in metazoans with four transmembrane domains, N- and C-terminal short intracellular domains, two extracellular loops and one short intracellular turn. Among several protein families with four transmembrane domains, tetraspanins are characterized especially by the structure of the second extracellular loop. It contains a highly conserved cysteine–cysteine–glycine (CCG) motif and two to four other cysteine residues. These cysteines form two or three disulfide

Journal of Cell Science (2016) 129, 1155-1164 doi:10.1242/jcs.180448

bonds within the loop (Charrin et al., 2014, 2009; Hemler, 2005; Yanez-Mo et al., 2009). Tetraspanins are believed to play a role in membrane compartmentalization and are involved in many biological processes, including cell migration, cell fusion and lymphocyte activation, as well as viral and parasitic infections (Charrin et al., 2014, 2009; Hemler, 2005; Yanez-Mo et al., 2009). Several tetraspanins regulate cell–cell adhesion (Chattopadhyay et al., 2003; Ishibashi et al., 2004; Shigeta et al., 2003) but none are known to be involved in the formation of epithelial occluding junctions. In the *Drosophila* genome, there are 37 tetraspanin family members (Charrin et al., 2014; Fradkin et al., 2002; Hemler, 2005; Todres et al., 2000), and some have been characterized by genetic analyses. Lbm, CG10106 and CG12143 participate in synapse formation (Fradkin et al., 2002; Kopczynski et al., 1996). Sun associates with light-dependent retinal degeneration (Xu et al., 2004). TspanC8 subfamily members, including Tsp3A, Tsp86D and Tsp26D, are involved in the Notch-dependent developmental processes through the regulation of a transmembrane metalloprotease, ADAM10 (human ortholog of Kuz in *Drosophila*) (Dornier et al., 2012). However, the functions of most other *Drosophila* tetraspanins remain obscure.

Here, we identify a tetraspanin family protein, Tsp2A, as a newly identified molecular component of sSJs in *Drosophila*. We demonstrate that Tsp2A is required for sSJ formation and for the barrier function of *Drosophila* midgut. Tsp2A and two other sSJ-specific membrane proteins, Mesh and Ssk, show mutually dependent localizations at sSJs and form a complex with each other. Therefore, we conclude that Tsp2A cooperates with Mesh and Ssk to organize sSJs.

RESULTS

Tsp2A is an sSJ component

We previously identified Mesh as a molecular component of sSJs (Izumi et al., 2012). Because sSJs are located in the apicolateral region of the plasma membrane in endodermally derived epithelia, apicolateral localization of Mesh might be considered to indicate the occurrence of sSJs. To identify genes responsible for sSJ formation, we attempted to obtain *Drosophila* strains defective in the apicolateral accumulation of Mesh by a genetic screen of a chromosomal deficiency stock, Bloomington Deficiency Kit. Previously, it was reported that the formation of sSJs is completed at the end of embryogenesis, by late stage 17 in the midgut epithelia, and by early stage 17 in the OELP (Tepass and Hartenstein, 1994). Here, we observed apicolateral accumulation of Mesh in the stage 16 OELP, suggesting sSJ formation in the OELP commences during this stage (Fig. 1A, upper panel). Because most chromosomal deficiencies in the kit are embryonic lethal, we evaluated sSJ formation in our screen by immunofluorescence staining of the stage 16 OELP with an anti-Mesh antibody. We identified several deficiencies that caused a defect in the accumulation of Mesh in the region of sSJs in the OELP.

In the OELP of Df(1)BSC534 (deleted segment: 1D1-2A3), Mesh was distributed diffusely in the cytoplasm (Fig. 1A, lower panel). To more precisely identify the genomic region responsible for the phenotype, we investigated the Mesh distribution of other deficiencies overlapping with Df(1)BSC534. As Df(1)BSC709 (deleted segment: 1E4-2A1) and Df(1)Exel6227 (deleted segment: 1F3-2B1) OELP exhibited the phenotype of the cytoplasmic distribution of Mesh, the Df(1)BSC534 phenotype was mapped to the 1F3-2A1 interval (data not shown). Within the genomic region 1F3-2A1, we focused on the gene for Tsp2A (Fig. 1B) because a Flybase search revealed that it is highly expressed in the midgut and the Malpighian tubules (http://flybase.org/reports/FBgn0024361.html). The *Tsp2A* gene encodes a tetraspanin family protein (Fig. 1D) (Fradkin et al., 2002; Todres et al., 2000). To examine whether a lack of Tsp2A caused the cytoplasmic localization of Mesh, we expressed N-terminal EGFP-tagged Tsp2A (EGFP–Tsp2A) in Df(1)Exel6227 using *da*-GAL4 (Fig. 2C,C′, see below). Interestingly, apicolateral accumulation of Mesh in the OELP was recovered and EGFP–Tsp2A was colocalized with Mesh (Fig. 2C,C′) in EGFP–Tsp2A-induced Df(1)Exel6227, whereas Mesh remained in the cytoplasm in control Df(1)Exel6227 (Fig. 2D′). These observations strongly suggest that among the genes deleted in Df(1)Exel6227, *Tsp2A* is responsible for sSJ localization of Mesh, and that Tsp2A itself is a component of sSJs.

To determine the expression pattern and the subcellular localization of endogenous Tsp2A, we obtained two anti-Tsp2A antibodies raised against the C-terminal cytoplasmic region of Tsp2A. Immunofluorescence microscopic analyses revealed that both of the affinity-purified anti-Tsp2A antibodies labeled the apicolateral region of the OELP in late-stage embryos (Fig. 2A,E; Fig. S1C,G). The staining pattern of the OELP with these antibodies distinctly overlapped that of an anti-Mesh antibody (Fig. 2A,A′,E–E″; Fig. S1C–C″,G–G″). Furthermore, the immunoreactivities of these antibodies in the OELP were diminished in Df(1)Exel6227 (Fig. 2B) and in *Tsp2A* mutant embryos (Fig. S1D,H, see below), indicating the specificity of these anti-Tsp2A antibodies. Immunofluorescence staining of first-instar larvae with one of the anti-Tsp2A antibodies revealed strong honeycomb-like signals of Tsp2A in the midgut, OELP and Malpighian tubules, but not in the foregut and hindgut (Fig. 2F,G). At higher magnification, the staining with the anti-Tsp2A antibody overlapped well with that of the anti-Mesh antibody in apicolateral regions of the midgut epithelial cells (Fig. 2I–I″). The anti-Tsp2A antibody also labeled apicolateral regions of cell–cell contact in adult midgut epithelial cells (Fig. 2H), and coincided with staining with the anti-Mesh antibody in these regions (Fig. 2J–J″). Taken together, these observations indicate that Tsp2A is a component of sSJs in *Drosophila* from the embryo to adulthood.

Tsp2A is required for proper organization of sSJ components

To confirm that Tsp2A is involved in the sSJ localization of Mesh, we induced *Tsp2A*-RNAi (11415R-2 generated by NIG-Fly) using *48Y*-GAL4 in wild-type larvae. In the *Tsp2A*-RNAi first-instar larvae, the levels of Tsp2A were decreased in the sSJs of the midgut epithelial cells and the OELP (Fig. 3B and data not shown). In these cells, Mesh was distributed diffusely in the cytoplasm (Fig. 3B′,F′; Fig. S2B′) and Ssk was mislocalized to the apical membrane, basolateral membrane and cytoplasm (Fig. 3F; Fig. S2B). These results indicate that Tsp2A is required for the sSJ localizations of Mesh and Ssk.

To further confirm the role of Tsp2A in the molecular organization of sSJs, we generated *Tsp2A* mutants using the CRISPR/Cas9 method provided by NIG-Fly (See Materials and Methods section) (Kondo and Ueda, 2013). We successfully obtained three independent *Tsp2A* mutant strains ($Tsp2A^{1\text{-}2}$, $Tsp2A^{2\text{-}9}$ and $Tsp2A^{3\text{-}3}$), all of which had small indel mutations encompassing the target site (Fig. 1C). These *Tsp2A* mutant embryos hatched into first-instar larvae but died at this stage (data not shown). Mutations in all *Tsp2A* mutants caused frameshifts and premature stop codons. Among these mutant strains, we mainly used $Tsp2A^{1\text{-}2}$ for further experiments. In western blot analysis, the anti-Tsp2A antibodies detected a large number of bands in the extracts of both wild-type and $Tsp2A^{1\text{-}2}$ first-instar larvae (Fig. S3A). Among them, only a ∼21 kDa band

Journal of Cell Science (2016) 129, 1155-1164 doi:10.1242/jcs.180448

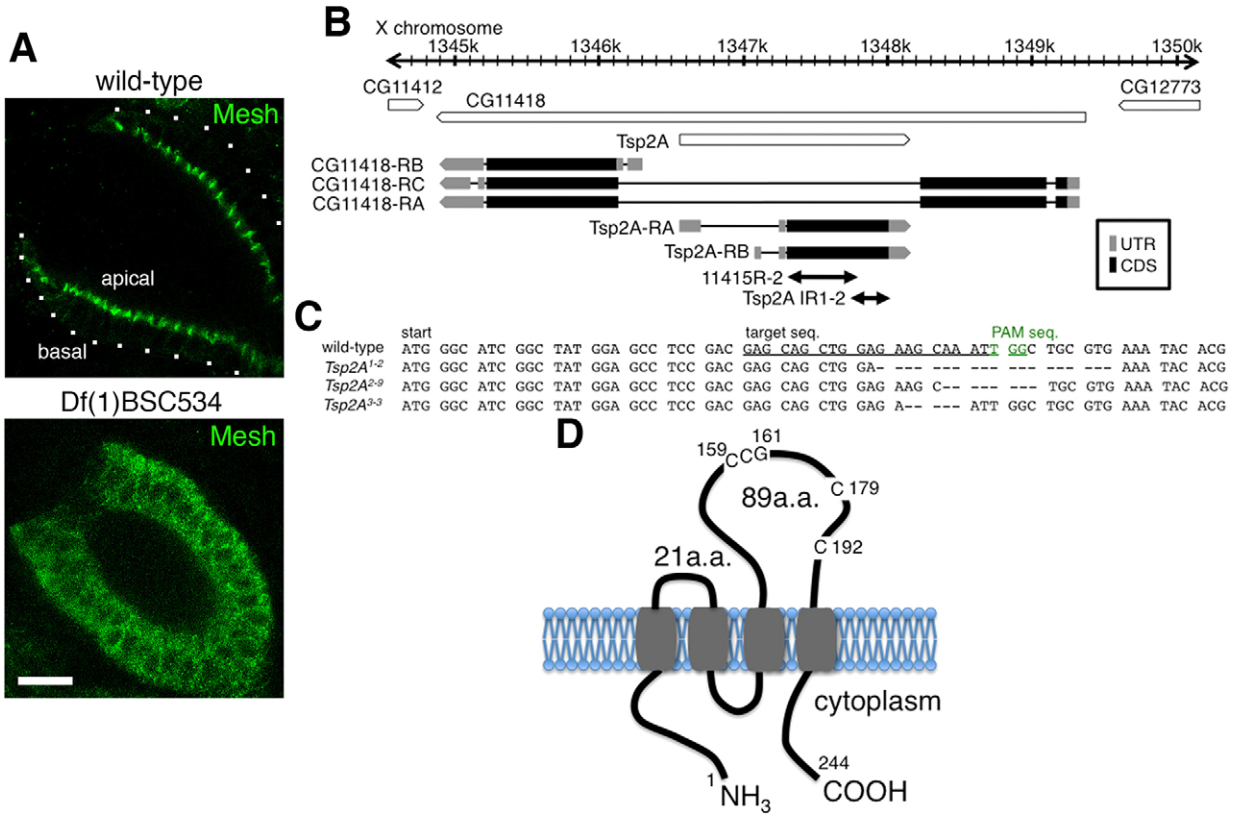

Fig. 1. Identification of *Tsp2A* as an sSJ-related gene by a deficiency screen. (A) Immunofluorescence staining of stage 16 wild-type and Df(1)BSC534 embryos using anti-Mesh antibody. Mesh is localized at sSJs of the OELP in the wild type but is distributed diffusely in the cytoplasm in Df(1)BSC534. Basal membranes are delineated by dots. Scale bar: 20 µm. (B) Physical map of the *Drosophila* X chromosome containing *Tsp2A* gene. Full-length genes of CG11418 and *Tsp2A* are contained in this region. They overlap but are encoded by the complementary DNA strands. The whole of *Tsp2A* is encoded within the region corresponding to the second intron of CG11418. The *Tsp2A* gene generates two transcripts, *Tsp2A*-RA and *Tsp2A*-RB, which share a common open reading frame. The *Tsp2A* DNA sequences used for the construction of *Tsp2A*-RNAi (11415R-2 and Tsp2A IR1-2) are indicated by lines with double arrowheads. Gray bar: untranslated regions of the *Tsp2A* transcript (UTR). Black bar: coding sequences of the *Tsp2A* transcripts (CDS). (C) Genomic sequences of *Tsp2A* mutations induced by the CRISPR/Cas9 method. The nucleotide sequence of wild-type *Tsp2A* from the start codon is shown at the top. The guide RNA target sequence is underlined and the PAM sequence is shown in green. Deleted nucleotides in the corresponding genome region in three *Tsp2A* mutants (*Tsp2A*$^{1-2}$, *Tsp2A*$^{2-3}$ and *Tsp2A*$^{3-3}$) obtained by the CRISPR/Cas9 method are shown by dashes. (D) A membrane-spanning model of Tsp2A. Tsp2A is a tetraspanin family protein, which is an integral membrane protein with four transmembrane domains. Tsp2A has several conserved amino acids characteristic of tetraspanin family proteins, including a CCG motif and other cysteine residues within the second extracellular loop.

disappeared in *Tsp2A*$^{1-2}$ extracts (Fig. S3A), implying that the ∼21 kDa band represents Tsp2A and that the other bands commonly observed in both the wild type and the *Tsp2A*$^{1-2}$ mutants originated from cross-reactions of these antibodies. We also noticed that a ∼18 kDa band was detected by an anti-Tsp2A antibody (301) only in *Tsp2A*$^{1-2}$ extracts (Fig. S3A, left panel). The open reading frame of the Tsp2A gene has an in-frame ATG codon at the 94th nucleotide and it is likely that the ∼18 kDa band corresponds to a peptide translated from this ATG. Because the ATG codon at the 94th nucleotide is present in the coding region corresponding to the middle of the first transmembrane domain of Tsp2A, the peptide translated from this ATG might be nonfunctional because of an abnormal conformation. Consistently, anti-Tsp2A antibodies did not stain the sSJ region in first-instar larva of *Tsp2A*$^{1-2}$ mutants (Fig. 3C,D). In the *Tsp2A*$^{1-2}$ midgut and the OELP, Mesh was distributed diffusely in the cytoplasm of the epithelial cells (Fig. 3C′; Fig. S2C′) and Ssk was mislocalized to the apical and basolateral membranes and cytoplasm (Fig. 3G,H; Fig. S2C,D), as also observed in the *Tsp2A*-RNAi midgut (Fig. 3B′,F,F′; Fig. S2B,B′). *Tsp2A*$^{2-9}$ and *Tsp2A*$^{3-3}$ mutants showed the same phenotype (Fig. S2F–I‴). Other sSJ components, such as Lgl [also known as L(2)gl], Cora and FasIII (also known as Fas3), were also mislocalized in the *Tsp2A*-RNAi and *Tsp2A*$^{1-2}$ mutant midgut; Lgl was distributed along the basolateral membrane (Fig. S4D,G), Cora was partially localized to the apicolateral regions but also was distributed diffusely throughout the cytoplasm (Fig. S4E,H), and FasIII was observed as large aggregates in the apicolateral and apical plasma membrane regions (Fig. S4F,I). By contrast, Dlg was still localized at the apicolateral region in the RNAi and mutant midgut (Fig. 3B″,C″,D″,F″,G″,H″; Fig. S2B″,C″,D″,F″,G″,H″,I″), suggesting that Tsp2A does not play a major role in specifying the apical–basal polarity of epithelial cells. Taken together, these results indicate that Tsp2A is required for the proper localization of a number of sSJ components.

Western blot analyses revealed that the densities of the main bands of Ssk (∼15 kDa) and Mesh (∼90 kDa) were not notably changed in *Tsp2A*$^{1-2}$ mutant larva, compared with wild type (Fig. S3B,D). However, two minor bands of Mesh at ∼200 kDa in the wild type converged into a single band with the higher molecular mass in the *Tsp2A*$^{1-2}$ mutant (Fig. S3D). This suggests that some post-translational processing of Mesh is affected by the loss of Tsp2A, although it is unknown whether there are differences in the biochemical properties of the two bands of Mesh around 200 kDa.

Journal of Cell Science (2016) 129, 1155-1164 doi:10.1242/jcs.180448

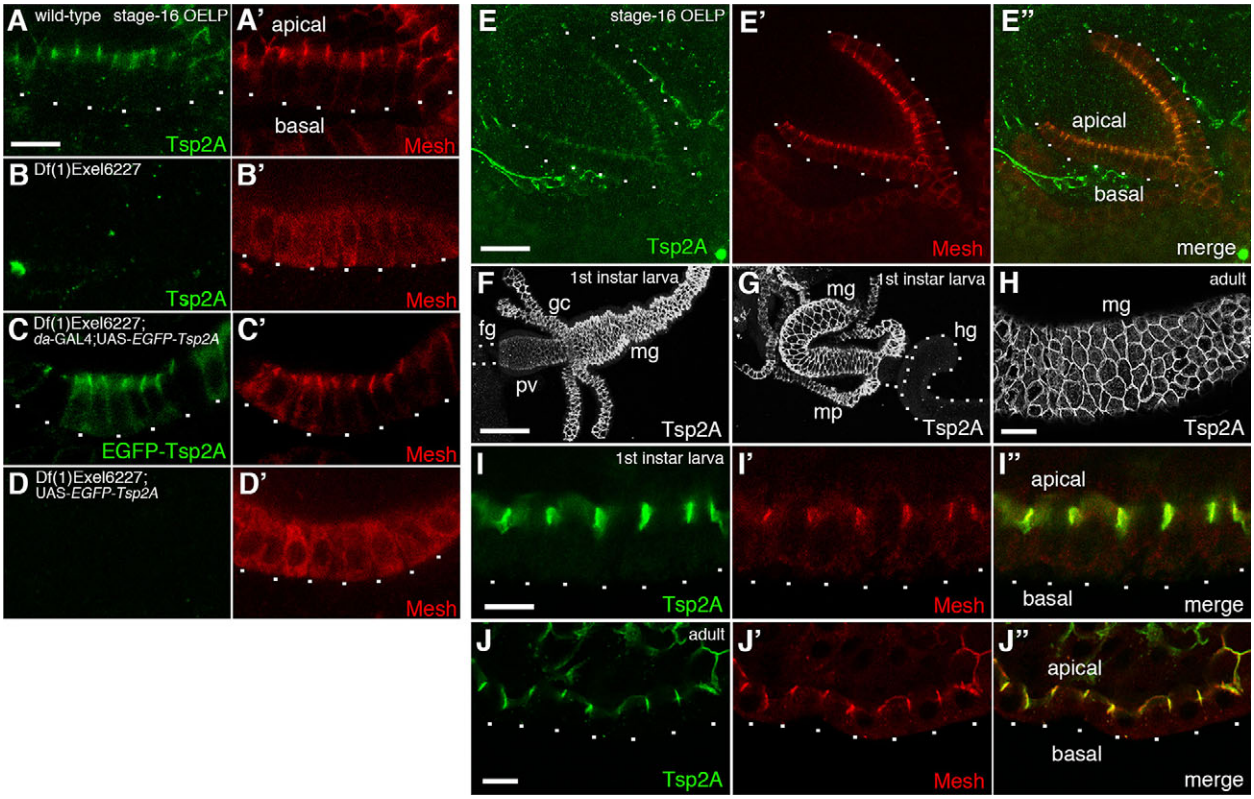

Fig. 2. Tsp2A localizes to sSJs. (A-D′) Double immunofluorescence staining of stage 16 wild-type (A,A′), Df(1)Exel6227 (B,B′), EGFP–Tsp2A-induced Df(1)Exel6227 [Df(1)Exel6227;*da*-GAL4;UAS-EGFP-Tsp2A] (C,C′) and control Df(1)Exel6227 [Df(1)Exel6227; UAS-EGFP-Tsp2A] (D,D′) embryos using anti-Tsp2A (A,B), anti-GFP (C,D) and anti-Mesh (A′,B′,C′,D′) antibodies. In wild-type OELP, Tsp2A and Mesh are accumulated at sSJs (A,A′). In Df(1)Exel6227 OELP, the staining of Tsp2A is eliminated (B) and Mesh is distributed diffusely in the cytoplasm (B′). The accumulation of EGFP–Tsp2A to sSJs (C) and rescue of the sSJ localization of Mesh are observed in the EGFP–Tsp2A-induced Df(1)Exel6227 OELP (C′) but not in the uninduced OELP (D,D′). Basal membranes are delineated by dots. (E–E″) Double immunofluorescence staining of a stage 16 wild-type embryo using anti-Tsp2A (E) and anti-Mesh (E′) antibodies. Tsp2A colocalizes with Mesh at sSJs (E″). Basal membranes are delineated by dots. (F–H) Wild-type first-instar larvae stained with anti-Tsp2A antibody in the anterior midgut (F), the posterior midgut (G) and the adult midgut (H). Tsp2A is expressed in the first-instar larval midgut, the OELP and the Malpighian tubules (F,G). In the adult midgut, it is localized in the epithelial cells at regions of cell–cell contact (H). Tsp2A signals are not detected in the foregut (F) or hindgut (G). fg, forgut; pv, proventriculus; gc, gastric caeca; mg, midgut; mp, Malpighian tubules; hg, hindgut. (I–I″) Double immunofluorescence staining of the wild-type first-instar larval midgut using anti-Tsp2A (I) and anti-Mesh (I′) antibodies. Tsp2A colocalizes with Mesh at sSJs of the larval midgut (I″). Basal membranes are delineated by dots. (J–J″) Double immunofluorescence staining of the wild-type adult midgut using anti-Tsp2A (J) and anti-Mesh (J′) antibodies. Tsp2A colocalizes with Mesh at sSJs of the adult midgut (J″). Basal membranes are delineated by dots. Scale bar: 5 µm in A–D′; 20 µm in E–E″; 50 µm in F,G; 50 µm in H; 5 µm in I–I″; 10 µm in J–J″.

To examine whether the role of Tsp2A is specific to sSJs, we observed the localization of the pSJ components, Kune and Cora, in the ectodermally derived epithelial cells in *Tsp2A*$^{1\text{-}2}$ mutants. In stage 16 embryos of both wild type and *Tsp2A*$^{1\text{-}2}$ mutants, Kune and Cora were found to be similarly localized within the apicolateral regions of the hindgut, epidermis and the salivary gland (Fig. S4J–K″ and data not shown), indicating that Tsp2A does not influence the organization of pSJs.

Tsp2A is required for the initial assembly of sSJs

We next examined the Tsp2A distribution during the sSJ formation process by immunofluorescence staining of wild-type embryos from stage 15 to stage 16. In the OELP of stage 15 embryos, Tsp2A was localized in aggregations along the lateral membranes (Fig. S1A,A″,E,E″) and accumulated into the apicolateral plasma membrane region in the stage 16 OELP, suggesting that Tsp2A is incorporated into the sSJs at stage 16 (Fig. S1C,C″,G,G″). These signals are specific for Tsp2A, because they were diminished in *Tsp2A* mutants (Fig. S1B,D,F,H). By contrast, Mesh was localized along the lateral membranes with partial accumulation in the apicolateral region in the stage 15 OELP, but did not form aggregates (Fig. S1A′,A″,E′,E″). In the stage 16 OELP, Mesh accumulated in the apicolateral regions and colocalized with Tsp2A (Fig. S1C′,C″,G′,G″). Thus, the sSJ targeting process of Tsp2A seems to differ from that of Mesh.

To test whether the *Tsp2A*$^{1\text{-}2}$ mutation affects the assembly or maintenance of sSJs, we monitored the distribution of Mesh during sSJ maturation in wild-type and *Tsp2A*$^{1\text{-}2}$ embryos. In the wild-type OELP, Mesh began to localize in the apicolateral region at stage 15 (Fig. S1A′,E′), and exclusively accumulated at sSJs at stage 16 (Fig. S1C′,G′). By contrast, in the *Tsp2A*$^{1\text{-}2}$ OELP, Mesh was distributed diffusely in the cytoplasm from stage 15 to stage 16 (Fig. S1B′,D′,F′,H′). Taken together, these results suggest that Tsp2A is required for the initial assembly of sSJs.

Tsp2A is required for proper sSJ structure

To investigate the role of Tsp2A in sSJ formation, the ultrastructure of the first-instar larval midgut in *Tsp2A*$^{1\text{-}2}$ mutants was examined by electron microscopy of ultrathin sections. In wild-type midgut epithelial cells, sSJs were observed as parallel plasma membranes between adjacent cells with ladder-like septa in the apicolateral regions of cell–cell contacts (Fig. 4A–D). In the *Tsp2A*$^{1\text{-}2}$ mutant, two types of defects were observed in the ultrastructure of the apicolateral regions of cell–cell contacts. First, septa-like structures

Journal of Cell Science (2016) 129, 1155-1164 doi:10.1242/jcs.180448

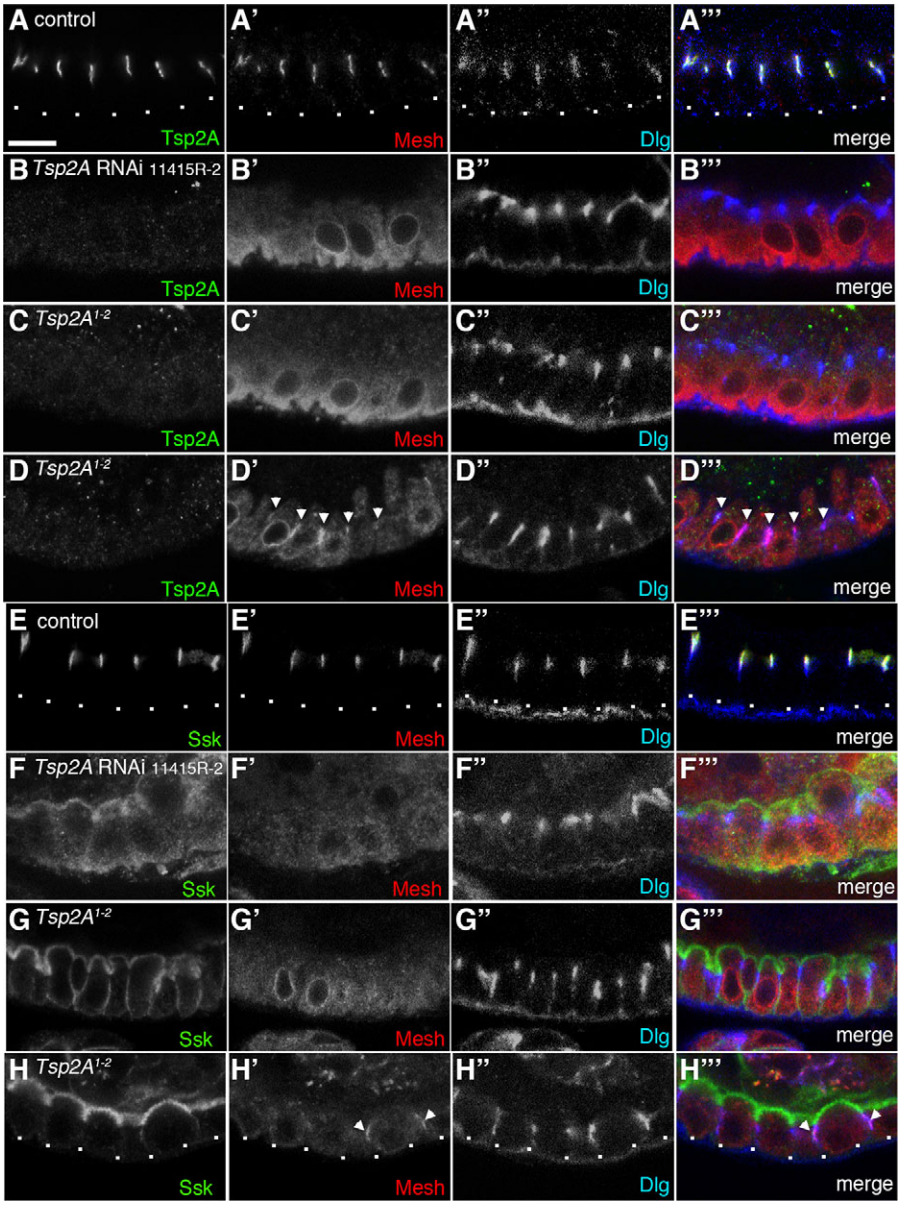

Fig. 3. Tsp2A is required for the localization of sSJ components. (A–D‴) The first-instar larval midgut of control (A–A‴), *Tsp2A*-RNAi 11415R-2 (B–B‴) and *Tsp2A*$^{1-2}$ (C–C‴,D–D‴) stained with anti-Tsp2A (A–D, green in merge), anti-Mesh (A′–D′, red in merge) and anti-Dlg (A″–D″, blue in merge) antibodies. The merged images are shown in A‴–D‴. Arrowheads in D′ and D‴ indicate the apicolateral localization of Mesh in *Tsp2A*$^{1-2}$ epithelial cells. (E–H‴) The first-instar larval midgut of control (E–E‴), *Tsp2A*-RNAi 11415R-2 (F–F‴) and *Tsp2A*$^{1-2}$ (G–G‴,H–H‴) stained with anti-Ssk (E–H, green in merge), anti-Mesh (E′–H′, red in merge) and anti-Dlg (E″–H″, blue in merge) antibodies. The merged images are shown in E‴–H‴. Arrowheads in H′ and H‴ indicate the apicolateral localization of Mesh in *Tsp2A*$^{1-2}$ epithelial cells. In the control midgut, Tsp2A, Mesh, Ssk and Dlg localize at sSJs (A–A‴,E–E‴). *Tsp2A*-RNAi (11415R-2 generated by NIG-FLY) induced by *48Y*-GAL4 on wild-type background decreases the level of Tsp2A at sSJs in the midgut of first-instar larvae (B). In these midgut epithelial cells, Mesh is distributed diffusely in the cytoplasm (B′,F′) and Ssk is mislocalized to the apical membrane, basolateral membrane and cytoplasm (F). In the *Tsp2A*$^{1-2}$ midgut, Tsp2A is not observed in the sSJ regions (C,D), Mesh is distributed diffusely in the cytoplasm (C′,G′) and Ssk is mislocalized to the apical and basolateral membranes (G). Dlg is still localized at the apicolateral region in *Tsp2A*-RNAi 11415R-2 and *Tsp2A*$^{1-2}$ midgut (B″,C″,D″,F″,G″,H″). In *Tsp2A*$^{1-2}$, Mesh (D,D‴,H′,H‴) and Ssk (H,H‴) are occasionally localized to the apicolateral region of the epithelial cells (D‴,H‴, arrowheads). The extent of the distributions of Ssk to the apical and basolateral membrane domains in *Tsp2A*$^{1-2}$ midgut epithelial cells varied among samples (G,H). Basal membranes are delineated by dots. Scale bar: 5 µm.

were occasionally visible but they were less electron-dense than the septa of sSJs in wild-type midgut (Fig. 4E–H), and the plasma membranes of adjacent cells were often more closely apposed than in the wild type (Fig. 4E). Second, large gaps were formed between the lateral membranes of adjacent cells (Fig. 4I–L). These results indicate that Tsp2A is required for proper sSJ formation at the ultrastructural level.

Tsp2A is required for the barrier function of the midgut

We next examined whether Tsp2A is involved in the barrier function of the midgut epithelium, as previously observed for Mesh and Ssk (Izumi et al., 2012; Yanagihashi et al., 2012). We designed a dye permeability assay, which analyzed leakage from the midgut to the body cavity of a fluorescent tracer taken with the food (Izumi et al., 2012; Yanagihashi et al., 2012). During the initial assay, we found that the *Tsp2A*-RNAi 11415R-2 first-instar larvae ate the food but the *Tsp2A* mutant larvae did not, although both animals died during the larval stage. Thus, we used the *Tsp2A*-RNAi 11415R-2 larvae for further experiments. Control first-instar larvae (+/UAS-*Tsp2A*-RNAi 11415R-2) and *Tsp2A*-RNAi 11415R-2 first-instar larvae (*48Y*-GAL4/UAS-*Tsp2A*-RNAi 11415R-2) were fed yeast containing fluorescently labeled dextran of 10 kDa and observed by confocal microscopy. In most control larvae, the midgut was well contrasted, with the fluorescent tracer confined within the midgut (Fig. 5A, upper panel and C). Conversely, the tracer was detected in various parts of the body cavity in a number of *Tsp2A*-RNAi 11415R-2 larvae (Fig. 5A, lower panel), indicating leakage of the tracer from the lumen of the midgut epithelium. In some *Tsp2A*-RNAi 11415R-2 larvae, the tracer was not detected in the body cavity, possibly caused by lower RNAi efficiency (Fig. 5C). To exclude off-target effects, we tested an additional RNAi line that targets a different sequence of the Tsp2A mRNA (Fig. 1B, Tsp2A IR1-2). In the *Tsp2A*-RNAi IR1-2 first-instar larvae (*48Y*-GAL4/UAS-*Tsp2A*-RNAi IR1-2), the levels of Tsp2A were decreased and the mislocalization of Mesh was observed in the midgut epithelial cells (Fig. S2J–J‴). Leakage of the tracer from the midgut was also observed in a number of *Tsp2A*-RNAi IR1-2 larvae but not in most control larvae (+/UAS-*Tsp2A*-RNAi IR1-2) (Fig. 5B). These observations indicate that Tsp2A is required for the barrier function of the midgut epithelium.

Journal of Cell Science (2016) 129, 1155-1164 doi:10.1242/jcs.180448

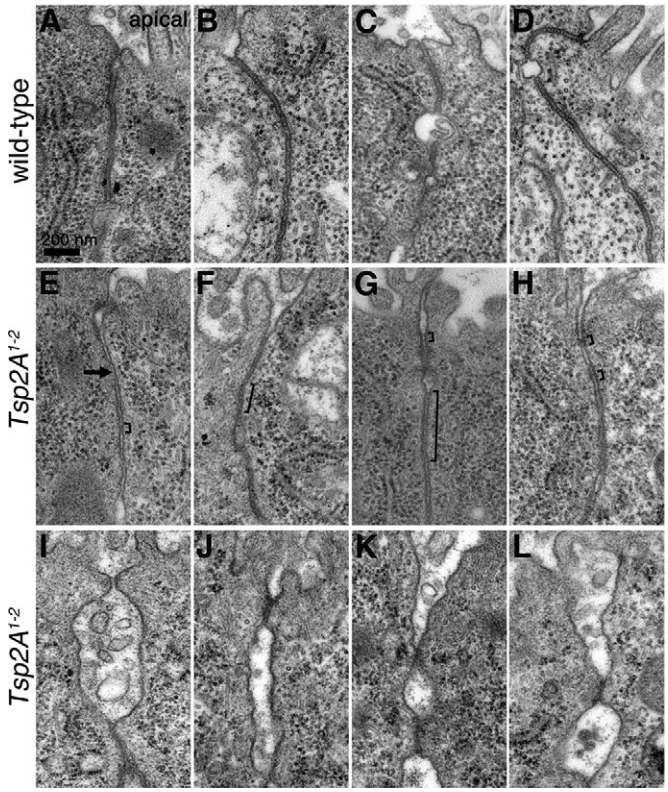

Fig. 4. Tsp2A is required for sSJ organization. (A–L) Transmission electron microscopy of the first-instar larval midgut in wild type (A–D) and *Tsp2A*$^{1-2}$ mutants (E–L). In the wild-type midgut, typical sSJs were observed at bicellular contacts (A–D). In the *Tsp2A*$^{1-2}$ mutant, two types of defects were observed in the apicolateral regions of cell–cell contacts. First, septa-like structures were occasionally visible but were less electron-dense than the septa of sSJs in wild-type midgut (E–H, brackets), and the plasma membranes of adjacent cells were often more closely apposed than the wild type (E, arrow). Second, large gaps were formed between the lateral membranes of adjacent cells (I–L). Scale bar: 200 nm.

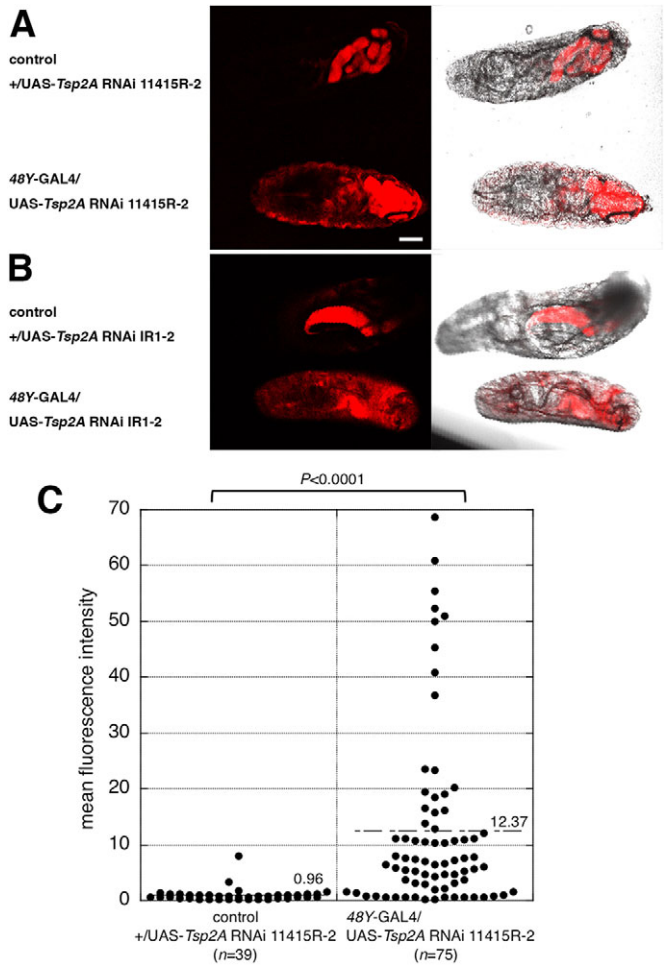

Fig. 5. Tsp2A is required for the barrier functions of the midgut. (A,B) Dye permeability assays using *Tsp2A*-RNAi induced by *48Y*-GAL4. Control first-instar larvae (A; +/UAS-*Tsp2A* RNAi 1145R-2 and B; +/UAS-*Tsp2A* RNAi IR1-2) and *Tsp2A*-RNAi first-instar larvae (A; *48Y*-GAL4/UAS-*Tsp2A*-RNAi 1145R-2 and B; *48Y*-GAL4/UAS-*Tsp2A*-RNAi IR1-2) were fed with Alexa-Fluor-555-labeled dextran (10 kDa). A typical fluorescent microscopic image containing both of the larvae in the same visual field (A,B; left panel) and merged with brightfield to trace the shape of larvae (A,B; right panel) are shown. In the control larva, the midgut is densely stained with the fluorescent tracer, which is confined within the midgut. The tracer is visible in various parts of the body cavity in the *Tsp2A*-RNAi larva. Scale bar: 100 µm. (C) Dot-plots showing mean Alexa-Fluor-555-labeled dextran fluorescence intensity in the most anterior part (area of the circle: 1232.783 µm^2) of the body cavity in individual larva. Bars and the numbers in the graph display the mean fluorescence intensity of the control or Tsp2A RNAi 11415R-2 larva. Statistical significance (P<0.0001) was determined by the Mann–Whitney U-test.

Tsp2A, Mesh and Ssk are mutually dependent for their sSJ localization

Because Mesh and Ssk were mislocalized in *Tsp2A*-deficient midgut epithelial cells, we next investigated whether the localization of Tsp2A is affected by loss of Mesh or Ssk. In most *mesh*^{f04955} mutant and Df(3L)ssk midgut epithelial cells, Tsp2A failed to localize to the apicolateral region but was distributed diffusely and formed aggregates in the cytoplasm (Fig. 6B,D), indicating that both Mesh and Ssk are required for the sSJ localization of Tsp2A. These observations, together with our previous report that Mesh and Ssk are interdependent for their localization (Izumi et al., 2012), indicate that the three sSJ-specific components, Tsp2A, Mesh and Ssk, are mutually dependent on each other for their proper localization, and work together to organize sSJs.

We noted that, whereas Tsp2A co-localized 100% with Dlg-positive apicolateral regions in wild type (n=234), this colocalization was reduced to 7.9% (n=202) in *mesh*^{f04955} mutant and 1.3% in Df(3L)ssk (n=225) epithelial cells (Fig. 6C-C″ and E-E″). Furthermore, we also observed a reduction in the accumulation of Mesh at the apicolateral regions where Dlg was localized from 100% in wild-type (n=202) to 3.2% in *Tsp2A*$^{1-2}$ (n=245) midgut epithelial cells (Fig. 3D′–D‴,H′–H‴; Fig. S2D′–D‴, G′–G‴ and I′–I‴). These observations suggest that although reduced, Tsp2A and Mesh do not completely lose the ability to accumulate in the apicolateral regions, even in the absence of other sSJ components.

Tsp2A forms a complex with Mesh and Ssk

The interdependency between Tsp2A, Mesh and Ssk for their localization at sSJs prompted us to examine whether Tsp2A is physically associated with Mesh and Ssk. Because we failed to immunoprecipitate endogenous Tsp2A with our anti-Tsp2A antibodies from the wild-type embryo in a range of conditions (data not shown), the embryos expressing EGFP–Tsp2A with *da*-GAL4 driver were subjected to immunoprecipitation with anti-GFP antibodies. When we used a lysis buffer

Journal of Cell Science (2016) 129, 1155-1164 doi:10.1242/jcs.180448

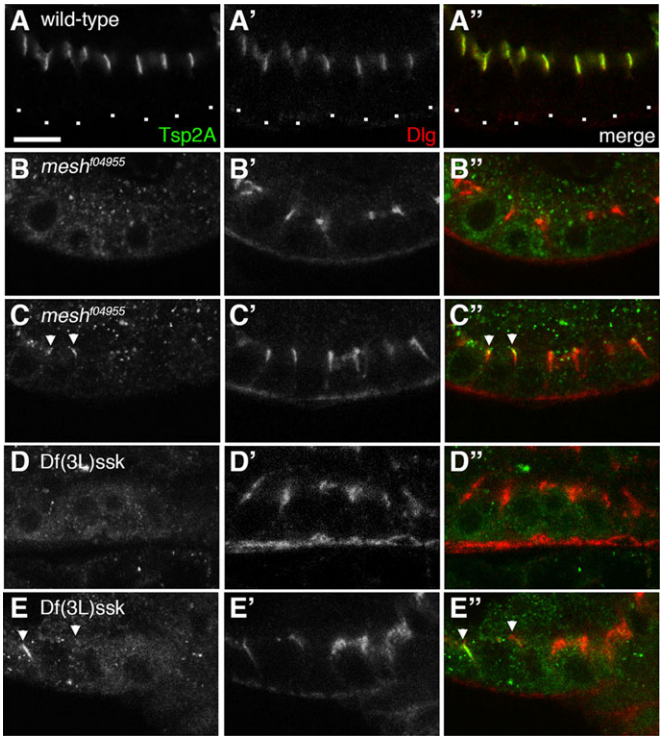

Fig. 6. Mesh and Ssk are required for sSJ localization of Tsp2A. (A–E″) The first-instar larval midgut of wild type, *mesh*^{f04955} mutant and Df(3L)ssk stained with anti-Tsp2A (A–E, green in merge) and anti-Dlg (A′–E′, red in merge) antibodies. The merged images are shown in A″–E″. Arrowheads in C,C″,E,E″ indicate the apicolateral localization of Tsp2A in *mesh*^{f04955} mutant and Df(3L)ssk epithelial cells. In the wild-type midgut, Tsp2A colocalizes with Dlg in the sSJs (A–A″). In the *mesh*^{f04955} mutant and Df(3L)ssk midguts, Tsp2A is distributed diffusely and forms some aggregates in the cytoplasm (B,D). Dlg is still localized at the apicolateral region in the *mesh*^{f04955} mutant and Df(3L)ssk midgut (B′,C′,D′,E′). In *mesh*^{f04955} mutant and Df(3L)ssk, Tsp2A is occasionally localized to the apicolateral region of midgut epithelial cells (C′,C″,E′,E″; arrowheads). Basal membranes are delineated by dots in A–A″. Scale bar: 5 µm.

containing NP-40 as a non-ionic detergent, EGFP–Tsp2A was immunoprecipitated with the anti-GFP antibodies, but co-precipitation of Ssk and Mesh with EGFP–Tsp2A was not detected (data not shown). Previous reports have shown that co-immunoprecipitation of tetraspanins with other tetraspanins or their partner integral membrane proteins depends on the detergents included in the lysis buffers (Charrin et al., 2009; Haining et al., 2012; Hemler, 2005; Yanez-Mo et al., 2009). Thus, the embryos expressing EGFP–Tsp2A were lysed with a buffer containing the non-ionic detergent Brij97, which has often been used in co-precipitation experiments in tetraspanin studies, and were subjected to immunoprecipitation with two anti-GFP antibodies. Western blot analysis of both of the precipitates with an anti-GFP antibody or the anti-Tsp2A antibodies specifically detected identical protein bands, indicating successful immunoprecipitation of EGFP–Tsp2A (Fig. 7A; Fig. S3E). Furthermore, co-precipitation of Mesh and Ssk with EGFP–Tsp2A was detected in these precipitated samples under these conditions (Fig. 7B). Neither Mesh nor Ssk was precipitated from EGFP–Tsp2A-expressing embryos with the control IgG, or from EGFP-expressing embryos with the anti-GFP antibody (Fig. 7B). Taken together, these results indicate that Tsp2A forms a complex with Mesh and Ssk *in vivo*.

DISCUSSION

We have identified a tetraspanin family protein, Tsp2A, as a newly discovered member of the sSJ-specific proteins. Tsp2A is required for sSJ formation and for the paracellular diffusion barrier in *Drosophila* midgut. Tsp2A forms a complex with Mesh and Ssk and cooperates with them to form sSJs. This study is the first demonstration that a tetraspanin family protein is required for the formation of an epithelial occluding junction.

The role of Tsp2A in sSJ formation

Of the sSJ-specific components, Mesh is a membrane-spanning protein and has an ability to induce cell–cell adhesion, implying that it is a cell adhesion molecule and might be one of the components of the electron-dense ladder-like structures in sSJs (Izumi et al., 2012). By contrast, both Ssk and Tsp2A are unlikely to act as cell adhesion molecules in sSJs because each of the two extracellular loops of Ssk (25 and 22 amino acids, respectively) appear to be too short to bridge the 15–20-nm intercellular space of sSJs (Lane et al., 1994; Tepass and Hartenstein, 1994). Furthermore, overexpression of EGFP–Tsp2A in *Drosophila* S2 cells did not induce cell aggregation, which is a criterion for cell adhesion activity (data not shown). Several observations in *Tsp2A* mutants might provide clues for understanding the role of Tsp2A in sSJ formation. In most *Tsp2A* mutant midgut epithelial cells, Mesh fails to localize to the apicolateral membranes but was distributed in the cytoplasm, possibly to specific intracellular membrane compartments. To further examine where Mesh was localized in *Tsp2A* mutant cells, we double-stained the midgut with the anti-Mesh antibody and the antibodies against typical markers of various intracellular membrane compartments, including the Golgi apparatus (anti-GM130), early endosomes (anti-Rab5), recycling endosomes (anti-Rab11) and lysosomes (anti-LAMP1). However, we were unable to detect any overlap between staining by these markers and that of Mesh (data not shown). We found that the staining pattern in *Tsp2A* mutant midgut epithelial cells produced with the anti-KDEL antibody, which labels endoplasmic reticulum, was similar, although not identical, to that produced by the anti-Mesh antibody (data not shown). Interestingly, some tetraspanins are known to control the intracellular trafficking of their partners. For instance, a mammalian tetraspanin, CD81, is necessary for normal trafficking or for surface membrane stability of a phosphoglycoprotein, CD19, in lymphoid B cells (Shoham et al., 2003). The TspanC8 subgroup proteins, which all possess eight cysteine residues in their large extracellular domain, regulate the exit of a metalloproteinase, ADAM10/Kuz, from the ER and differentially control its targeting to either late endosomes or to the plasma membrane (Dornier et al., 2012; Haining et al., 2012; Prox et al., 2012). Consequently, TspanC8 proteins regulate Notch signaling through the activation of ADAM10/Kuz in mammals, *Drosophila* and *Caenorhabditis elegans* (Dornier et al., 2012; Dunn et al., 2010). If Mesh is retained in the trafficking pathway from endoplasmic reticulum to plasma membrane in *Tsp2A* mutant cells, Tsp2A might have an ability to promote the intracellular trafficking of Mesh in the secretory pathway. To clarify the role of Tsp2A in sSJ formation, it will be necessary to determine the intracellular membrane compartment where Mesh was localized in *Tsp2A* mutant cells.

We found that Tsp2A, Mesh and Ssk were mutually dependent for their localization at sSJs. Consistent with this intimate relationship, the co-immunoprecipitation experiment revealed that Tsp2A physically interacts with Mesh and Ssk *in vivo*. However, the amount of Ssk observed in the co-immunoprecipitation with EGFP–Tsp2A was barely enriched

Journal of Cell Science (2016) 129, 1155-1164 doi:10.1242/jcs.180448

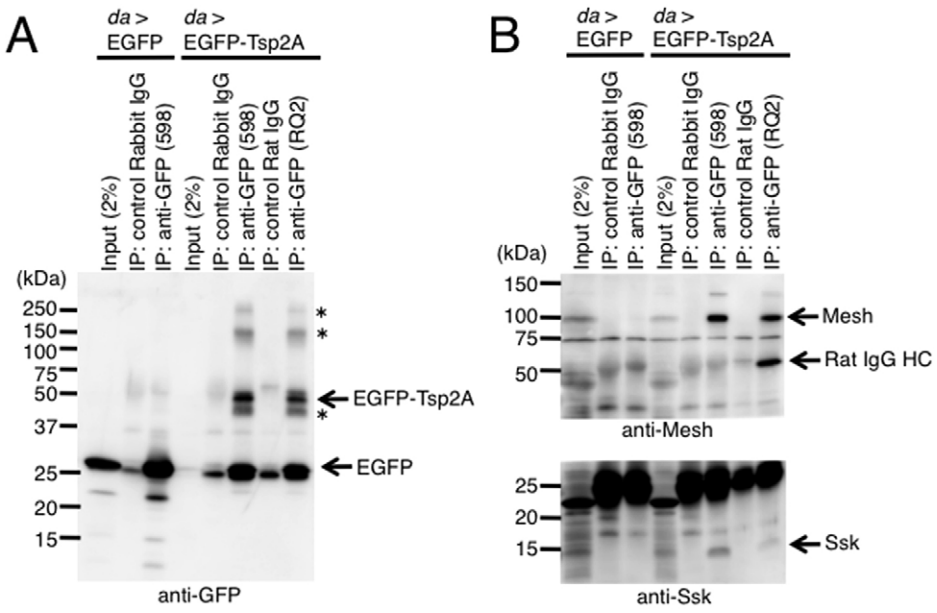

Fig. 7. Tsp2A forms a complex with Mesh and Ssk. Extracts of embryos expressing EGFP or EGFP–Tsp2A with *da*-GAL4 driver (Input) are subjected to immunoprecipitation (IP) with two kinds of anti-GFP antibodies (598 and RQ2). The immunocomplexes were separated on a 12% SDS-polyacrylamide gel, and western blot analyses were performed using anti-GFP (A), anti-Mesh (B; upper panel) or anti-Ssk (B; lower panel) antibodies. Immunoprecipitations of EGFP–Tsp2A (~50 kDa, arrow) with anti-GFP antibodies were detected when a buffer containing Brij97 was used to lyse embryos expressing EGFP–Tsp2A (A). In addition to the main band of EGFP–Tsp2A (arrow), weak bands at 250, 150, and 40 kDa are visible (asterisks). These bands are also recognized by anti-Tsp2A antibody (Fig. S3E) (A). EGFP is immunoprecipitated with anti-GFP antibodies from the embryos expressing EGFP (A). Mesh (B, upper panel) and Ssk (B, lower panel) are co-precipitated with EGFP–Tsp2A. Neither Mesh nor Ssk is precipitated with the control IgG from embryos expressing EGFP–Tsp2A (B). In the input lane of the embryos expressing EGFP–Tsp2A, the specific bands of EGFP–Tsp2A were undetectable by the anti-GFP antibody (A).

relative to the total amount detected in extracts of embryos expressing EGFP–Tsp2A. This was particularly striking in comparison to the degree of enrichment of Mesh in the co-immunoprecipitation with EGFP–Tsp2A. To interpret these results, we need to further clarify the detailed manner of the interaction between Tsp2A, Mesh and Ssk proteins. Many tetraspanin family proteins are known to interact with one another and with other integral membrane proteins to form a dynamic network of proteins in cellular membranes. Tetraspanins are also believed to have a role in membrane compartmentalization (Charrin et al., 2014, 2009; Hemler, 2005; Yanez-Mo et al., 2009). Given such functional properties of tetraspanins, Tsp2A might determine the localization of sSJs at the apicolateral membrane region by membrane domain formation.

In the *Tsp2A* mutant midgut epithelial cells, Lgl was distributed throughout the basolateral membrane region, whereas it was localized in the apicolateral membrane region in the wild type. In view of the role of Lgl in the formation of the apical–basal polarity of ectodermally derived epithelial cells, it is of interest to consider whether this abnormal localization of Lgl in the *Tsp2A* mutant affects epithelial polarity. However, in the *Tsp2A* mutant midgut epithelial cells, Dlg still showed polarized concentration into the apicolateral membrane region and Lgl did not leak into the apical membrane domain. These observations suggest that the lack of Tsp2A does not affect the gross apical–basal polarity of the midgut epithelial cells.

Tetraspanins and cell–cell junctions

Some tetraspanins have been reported to be involved in the regulation of cell–cell adhesion (Chattopadhyay et al., 2003; Ishibashi et al., 2004; Shigeta et al., 2003). A mammalian tetraspanin, CD151, regulates epithelial cell–cell adhesion through PKC- and Cdc42-dependent actin reorganization (Shigeta et al., 2003), or through complex formation with α3β1 integrin (Chattopadhyay et al., 2003). A mammalian tetraspanin, CD9, is concentrated in the axoglial paranodal region in the brain and in the peripheral nervous system, and CD9 knockout mice display defects in the formation of paranodal septate junctions and in the localization of paranodal proteins (Ishibashi et al., 2004). Paranodal septate junctions have electron-dense ladder-like structures and their molecular organization is similar to that of pSJs, but tetraspanins involved in pSJ formation have not been reported in *Drosophila*.

Interactions between several tetraspanins and claudins, the key integral membrane proteins involved in the organization and function of tight junctions, are also known. Claudin-11 forms a complex with OAP-1/Tspan-3 (Tiwari-Woodruff et al., 2001) and chemical crosslinking reveals a direct association between claudin-1 and CD9 (Kovalenko et al., 2007). Furthermore, the interaction between claudin-1 and CD81 is shown to be required for hepatitis C virus infectivity (Evans et al., 2007). To date, no tight junction defect has been reported in CD9 knockout mice, CD81 knockout mice, or CD9/CD81 double knockout mice (Charrin et al., 2014, 2009; Hemler, 2005; Takeda et al., 2003; Yanez-Mo et al., 2009). Further investigation is necessary to clarify whether the interactions between tetraspanins and tight-junction proteins are involved in the formation and function of tight junctions.

MATERIALS AND METHODS

Fly stocks and genetics

The fly strains *mesh*^{f04955}, *da*-GAL4 and *48Y*-GAL4 were obtained from the Bloomington Stock Center, and the *Tsp2A*-RNAi strain 11415R-2 was obtained from NIG-Fly. We also used the strain Df(3L)ssk (Yanagihashi et al., 2012). For the phenotype rescue experiment, pUAST vectors (Brand

Journal of Cell Science (2016) 129, 1155-1164 doi:10.1242/jcs.180448

and Perrimon, 1993) containing *EGFP–Tsp2A* were constructed and a fly strain carrying this construct was established.

cDNA cloning and expression vector construction

The ORF of *Tsp2A*, including the initiation codon, was amplified by PCR with the forward primer with a *Bgl*II site (5′-gaagatctATGGGCATCGGC-TATGGAGC-3′) and the reverse primer with a *Kpn*I site (5′-ggggtaccTC-AGCGGCGGTAGTTGCTGG-3′) from *Drosophila* embryonic cDNA, and cloned into the *Bgl*II and *Kpn*I sites of pUAST vector (Brand and Perrimon, 1993). To generate an expression vector for N-terminal EGFP-tagged Tsp2A, EGFP cDNA lacking the stop codon with 3′ and 5′ *Bgl*II sites was cloned into the *Bgl*II site of pUAST-*Tsp2A*. To generate an RNAi line (Tsp2A IR1-2), a DNA fragment containing nucleotides 381 to 725 of the *Tsp2A* ORF was amplified by PCR with the forward primer with an *Eco*RI (5′-gaattcGCAGTTCAGCACTATCAACT-3′) or a *Kpn*I site (5′-ggtaccG-CAGTTCAGCACTATCAACT-3′), and the reverse primer with a *Bgl*I site (5′-agatctTAGTTGCTGGCCTGTTCCTC-3′). The two types of DNA fragment were inserted into pUAST as a head-to-head dimer and transformed into SURE2 competent cells (200152, Agilent Technologies, Santa Clara, CA, USA). Transgenic flies were generated by standard P-element transformation procedures.

Generation of Tsp2A mutants

Generation of Tsp2A mutants using the CRISPR/Cas9 system was performed according to the method described by Kondo and Ueda (2013). To construct a guide RNA (gRNA) expression vector for *Tsp2A*, two complementary 24-bp oligonucleotides of the target sequence with 4-bp overhangs on both ends (5′-cttcGAGCAGCTGGAGAAGCAAAT-3′ and 5′-aaacATTTGCTTCTCCAGCTGCTC-3′) were annealed to generate a double-strand DNA, and cloned into *Bbs*I-digested pBFv-U6.2 (pBFv-U6.2-*Tsp2A*CR1). pBFv-U6.2-*Tsp2A*CR1 was injected into the y^1 v^1 *nos-phiC31; attP40* host (Bischof et al., 2007). Surviving G_0 males were individually crossed to y^2 cho^2 v^1 virgins. A single male transformant from each cross was mated to y^2 cho^2 v^1*; Sp/CyO* virgins. Offspring in which the transgene was balanced were collected to establish a stock.

Females carrying a U6.2-*Tsp2A*CR1 transgene were crossed to *nos*-Cas9 males (y^2 cho^2 v^1*/Y; Sp/CyO, P{nos-Cas9}2A*) to obtain founder flies that have both the U6.2-*Tsp2A*CR1 and the *nos*-Cas9 transgenes. Female founders were crossed to FM7c/Y male flies. Each female possessing a y^2 cho^2 v^1*/FM7c; CyO, P{nos-Cas9}2A/+* genotype was crossed to FM7c/Y male flies and the offspring possessing a y^2 cho^2 v^1*/FM7c* genotype were collected to establish the lines. The embryos of the lethal lines were immunostained for Tsp2A. Genomic DNA of the Tsp2A-negative lines was extracted and analyzed for lesions on the *Tsp2A* gene locus.

Deficiency screen

Embryos of deficiency lines obtained from the Bloomington Stock Center and the *Drosophila* Genetic Resource Center (Kyoto, Japan) were stained for Mesh. The OELP in stage 16 embryos was observed to determine whether Mesh was mislocalized. In the first screen, more than 20 embryos of deficiency lines were observed and the candidate lines that showed mislocalization of Mesh were isolated. To confirm the mislocalization of Mesh observed in the candidate lines, their balancer chromosomes were replaced by β-galactosidase-expressing balancers and the β-galactosidase-negative embryos were assumed to be homozygous for the deficiency lines.

Production of polyclonal antibodies

To generate anti-Tsp2A polyclonal antibodies, a polypeptide corresponding to the C-terminal cytoplasmic domain (NH_2-CAVKKEEEQASNYRR-COOH) of Tsp2A was synthesized and coupled by means of the cysteine residue to keyhole limpet hemocyanin (Eurofins Genomics, Tokyo, Japan). Polyclonal antibodies were generated in rabbits (301 and 302) by Kiwa Laboratory Animals (Wakayama, Japan). Rabbit antisera were affinity purified by Sulfolink Immobilization Kit (44999, Thermo Fisher Scientific, Waltham, Massachusetts, USA) according to the manufacturer's instructions (301AP and 302AP).

Immunohistochemistry

Embryos were fixed with 3.7% formaldehyde in PBS for 20 min. Larvae were dissected in Hanks' Balanced Salt Solution and fixed with 3.7% formaldehyde in PBS-0.4% Triton X-100. The following antibodies were used: rabbit anti-Tsp2A (302AP, 1:200), rabbit anti-Mesh (955-1; 1:1000) (Izumi et al., 2012), rat anti-Mesh (8002; 1:500) (Izumi et al., 2012), rabbit anti-Ssk (6981-1; 1:1000) (Yanagihashi et al., 2012), mouse anti-Dlg [4F3, Developmental Studies Hybridoma Bank (DSHB); 1:50], mouse anti-Coracle (C615.16, DSHB; 1:50), mouse anti-Fasciclin III (7G10, DSHB; 1:20), rabbit anti-Lgl (provided by F. Matsuzaki, RIKEN CDB; 1:1000), rabbit anti-Kune (1:500) (Nelson et al., 2010). Alexa-Fluor-488-conjugated (A21206, Invitrogen), and Cy3- and Cy5-conjugated (712-165-153 and 715-175-151, Jackson ImmunoResearch Laboratories, West Grove, PA, USA) secondary antibodies were used at 1:400. For the Tsp2A staining in Fig. 6, the anti-Tsp2A antibody was pre-incubated with $Tsp2A^{1-2}$ first-instar larvae overnight at 4°C. Samples were mounted in Vectashield (H-1000, Vector Laboratories, Burlingame, CA, USA). Images were acquired with a confocal microscope (model TCS-SPE; Leica Microsystems, Wetzlar, Germany) with its accompanying software using HC PLAN Apochromat 20× NA 0.7 and HCX PL Apochromat 63× NA 1.4 objective lenses (Leica Microsystems). Images were processed with Adobe Photoshop.

Electron microscopy

First-instar larvae of wild type or *Tsp2A* mutants were dissected and fixed overnight at 4°C with a mixture of 2.5% glutaraldehyde and 2% paraformaldehyde in 0.1 M cacodylate buffer (pH 7.4). The specimens, including the midguts, were prepared as described previously (Izumi et al., 2012). Ultrathin sections (50–100 nm) were stained doubly with 4% hafnium (IV) chloride and lead citrate, and observed with a JEM-1010 electron microscope (JEOL, Tokyo, Japan) equipped with Velete TEM CCD Camera (Olympus, Tokyo, Japan) at an accelerating voltage of 80 kV.

Co-immunoprecipitation and western blotting

Fly embryos expressing EGFP–Tsp2A or GFP (*da*-Gal4>UAS-EGFP-Tsp2A or UAS-GFP) were mixed with a 5-fold volume of lysis buffer [30 mM Tris-HCl pH 7.5, 150 mM NaCl, 1% Brij97 (P6136, Sigma-Aldrich, St. Louis, MO, USA)] and protease inhibitor cocktail (25955-11, Nakarai Tesque, Kyoto, Japan) and homogenized using a pestle for 1.5 ml microfuge tubes. The method for immunoprecipitation was essentially the same as described previously (Izumi et al., 2012). Rabbit anti-GFP (598, MBL, Nagoya, Japan) and rat anti-GFP (RQ2, MBL and GF090R, Nakarai Tesque) antibodies were used for immunoprecipitation. Immunocomplexes and extracts of the first-instar larva were separated on SDS-polyacrylamide gels, transferred to polyvinylidene difluoride membranes and western blot analyses were performed using mouse anti-GFP (clone 7.1+13.1, Roche, Basel, Switzerland; 1:500), rabbit anti-Tsp2A (301AP and 302AP; 1:200), rabbit anti-Ssk (6981-1; 1:1000), rat anti-Mesh (8002; 1:500) and mouse anti-α-tubulin (DM-1A; 1:1000, Sigma-Aldrich) antibodies.

Dye feeding experiments

Embryos (1–15 h after laying) were put on yeast paste containing Alexa-Fluor-555-labeled dextran (MW 10,000; Thermo Fisher Scientific) to feed newly hatched larvae. After 10–15 h, first-instar larvae were washed with water. Images were acquired with a confocal microscope (model TCS-SPE; Leica Microsystems) and its accompanying software using an HC PLAN Apochromat 10× NA 0.3 objective lens (Leica Microsystems). Images were processed with Adobe Photoshop. Mean Alexa-Fluor-555-labeled dextran-derived fluorescence intensity in the most anterior part (area of the circle: 1232.783 μm^2) of the body cavity in individual larva was quantified using Image J software (National Institutes of Health, MD, USA). Mean fluorescence intensity was taken as the read-out value. Statistical significance was evaluated by the Mann–Whitney *U*-test (KaleidaGraph, Synergy Software).

Acknowledgements

We are grateful to S. Yonemura, A. Nagafuchi and all the members of Furuse laboratories for helpful discussions. We also thank F. Matsuzaki for the antibody and the fly stocks, and the Bloomington Stock Center, the Drosophila Genetic Resource

Center at Kyoto Institute of Technology and the fly stocks of National Institute of Genetics (NIG-Fly) for fly stock.

Competing interests
The authors declare no competing or financial interests.

Author contributions
Y.I. and M.F. designed research; Y.I., M.M. and K.F. performed the experiments; Y.I. analyzed data; Y.I. and M.F. wrote the paper.

Funding
This work is supported by the Funding Program for Next Generation World Leading Researchers [grant number LS084] to M.F. and Grants-in-Aid for Scientific Research (C) [grant number 15612750] to Y.I. from the Japan Society for the Promotion of Science.

Supplementary information
Supplementary information available online at
http://jcs.biologists.org/lookup/suppl/doi:10.1242/jcs.180448/-/DC1

References
Anderson, J. M. and Van Itallie, C. M. (2009). Physiology and function of the tight junction. *Cold Spring Harb. Perspect. Biol.* **1**, a002584.

Banerjee, S., Sousa, A. D. and Bhat, M. A. (2006). Organization and function of septate junctions: an evolutionary perspective. *Cell Biochem. Biophys.* **46**, 65-77.

Bischof, J., Maeda, R. K., Hediger, M., Karch, F. and Basler, K. (2007). An optimized transgenesis system for *Drosophila* using germ-line-specific phiC31 integrases. *Proc. Natl. Acad. Sci. USA* **104**, 3312-3317.

Brand, A. H. and Perrimon, N. (1993). Targeted gene expression as a means of altering cell fates and generating dominant phenotypes. *Development* **118**, 401-415.

Byri, S., Misra, T., Syed, Z. A., Batz, T., Shah, J., Boril, L., Glashauser, J., Aegerter-Wilmsen, T., Matzat, T., Moussian, B. et al. (2015). The triple-repeat protein Anakonda controls epithelial tricellular junction formation in *Drosophila*. *Dev. Cell* **33**, 535-548.

Charrin, S., le Naour, F., Silvie, O., Milhiet, P.-E., Boucheix, C. and Rubinstein, E. (2009). Lateral organization of membrane proteins: tetraspanins spin their web. *Biochem. J.* **420**, 133-154.

Charrin, S., Jouannet, S., Boucheix, C. and Rubinstein, E. (2014). Tetraspanins at a glance. *J. Cell Sci.* **127**, 3641-3648.

Chattopadhyay, N., Wang, Z., Ashman, L. K., Brady-Kalnay, S. M. and Kreidberg, J. A. (2003). α3β1 integrin-CD151, a component of the cadherin-catenin complex, regulates PTPμ expression and cell-cell adhesion. *J. Cell Biol.* **163**, 1351-1362.

Deligiannaki, M., Casper, A. L., Jung, C. and Gaul, U. (2015). Pasiflora proteins are novel core components of the septate junction. *Development* **142**, 3046-3057.

Dornier, E., Coumailleau, F., Ottavi, J.-F., Moretti, J., Boucheix, C., Mauduit, P., Schweisguth, F. and Rubinstein, E. (2012). TspanC8 tetraspanins regulate ADAM10/Kuzbanian trafficking and promote Notch activation in flies and mammals. *J. Cell Biol.* **199**, 481-496.

Dunn, C. D., Sulis, M. L., Ferrando, A. A. and Greenwald, I. (2010). A conserved tetraspanin subfamily promotes Notch signaling in *Caenorhabditis elegans* and in human cells. *Proc. Natl. Acad. Sci. USA* **107**, 5907-5912.

Evans, M. J., von Hahn, T., Tscherne, D. M., Syder, A. J., Panis, M., Wolk, B., Hatziioannou, T., McKeating, J. A., Bieniasz, P. D. and Rice, C. M. (2007). Claudin-1 is a hepatitis C virus co-receptor required for a late step in entry. *Nature* **446**, 801-805.

Fradkin, L. G., Kamphorst, J. T., DiAntonio, A., Goodman, C. S. and Noordermeer, J. N. (2002). Genomewide analysis of the *Drosophila* tetraspanins reveals a subset with similar function in the formation of the embryonic synapse. *Proc. Natl. Acad. Sci. USA* **99**, 13663-13668.

Furuse, M. and Tsukita, S. (2006). Claudins in occluding junctions of humans and flies. *Trends Cell Biol.* **16**, 181-188.

Green, C. R. and Bergquist, P. R. (1982). Phylogenetic relationships within the invertebrata in relation to the structure of septate junctions and the development of occluding junctional types. *J. Cell Sci.* **53**, 279-305.

Haining, E. J., Yang, J., Bailey, R. L., Khan, K., Collier, R., Tsai, S., Watson, S. P., Frampton, J., Garcia, P. and Tomlinson, M. G. (2012). The TspanC8 subgroup of tetraspanins interacts with A disintegrin and metalloprotease 10 (ADAM10) and regulates its maturation and cell surface expression. *J. Biol. Chem.* **287**, 39753-39765.

Hemler, M. E. (2005). Tetraspanin functions and associated microdomains. *Nat. Rev. Mol. Cell Biol.* **6**, 801-811.

Hildebrandt, A., Pflanz, R., Behr, M., Tarp, T., Riedel, D. and Schuh, R. (2015). Bark beetle controls epithelial morphogenesis by septate junction maturation in *Drosophila*. *Dev. Biol.* **400**, 237-247.

Ishibashi, T., Ding, L., Ikenaka, K., Inoue, Y., Miyado, K., Mekada, E. and Baba, H. (2004). Tetraspanin protein CD9 is a novel paranodal component regulating paranodal junctional formation. *J. Neurosci.* **24**, 96-102.

Izumi, Y. and Furuse, M. (2014). Molecular organization and function of invertebrate occluding junctions. *Semin. Cell Dev. Biol.* **36**, 186-193.

Izumi, Y., Yanagihashi, Y. and Furuse, M. (2012). A novel protein complex, Mesh-Ssk, is required for septate junction formation in the *Drosophila* midgut. *J. Cell Sci.* **125**, 4923-4933.

Kondo, S. and Ueda, R. (2013). Highly improved gene targeting by germline-specific Cas9 expression in *Drosophila*. *Genetics* **195**, 715-721.

Kopczynski, C. C., Davis, G. W. and Goodman, C. S. (1996). A neural tetraspanin, encoded by late bloomer, that facilitates synapse formation. *Science* **271**, 1867-1870.

Kovalenko, O. V., Yang, X. H. and Hemler, M. E. (2007). A novel cysteine cross-linking method reveals a direct association between claudin-1 and tetraspanin CD9. *Mol. Cell. Proteomics* **6**, 1855-1867.

Lane, N. J. and Swales, L. S. (1982). Stages in the assembly of pleated and smooth septate junctions in developing insect embryos. *J. Cell Sci.* **56**, 245-262.

Lane, N. J., Dallai, R., Martinucci, G. and Burighel, P. (1994). Electron microscopic structure and evolution of epithelial junctions. In *Molecular Mechanisms of Epithelial Cell Junctions: From Development to Disease* (ed. S. Citi, R.G. Landes Co., USA), pp. 23-43.

Nelson, K. S., Furuse, M. and Beitel, G. J. (2010). The *Drosophila* Claudin Kune-kune is required for septate junction organization and tracheal tube size control. *Genetics* **185**, 831-839.

Prox, J., Willenbrock, M., Weber, S., Lehmann, T., Schmidt-Arras, D., Schwanbeck, R., Saftig, P. and Schwake, M. (2012). Tetraspanin15 regulates cellular trafficking and activity of the ectodomain sheddase ADAM10. *Cell. Mol. Life Sci.* **69**, 2919-2932.

Shigeta, M., Sanzen, N., Ozawa, M., Gu, J., Hasegawa, H. and Sekiguchi, K. (2003). CD151 regulates epithelial cell-cell adhesion through PKC- and Cdc42-dependent actin cytoskeletal reorganization. *J. Cell Biol.* **163**, 165-176.

Shoham, T., Rajapaksa, R., Boucheix, C., Rubinstein, E., Poe, J. C., Tedder, T. F. and Levy, S. (2003). The tetraspanin CD81 regulates the expression of CD19 during B cell development in a postendoplasmic reticulum compartment. *J. Immunol.* **171**, 4062-4072.

Takeda, Y., Tachibana, I., Miyado, K., Kobayashi, M., Miyazaki, T., Funakoshi, T., Kimura, H., Yamane, H., Saito, Y., Goto, H. et al. (2003). Tetraspanins CD9 and CD81 function to prevent the fusion of mononuclear phagocytes. *J. Cell Biol.* **161**, 945-956.

Tepass, U. and Hartenstein, V. (1994). The development of cellular junctions in the *Drosophila* embryo. *Dev. Biol* **161**, 563-596.

Tepass, U., Tanentzapf, G., Ward, R. and Fehon, R. (2001). Epithelial cell polarity and cell junctions in *Drosophila*. *Annu. Rev. Genet.* **35**, 747-784.

Tiwari-Woodruff, S. K., Buznikov, A. G., Vu, T. Q., Micevych, P. E., Chen, K., Kornblum, H. I. and Bronstein, J. M. (2001). OSP/claudin-11 forms a complex with a novel member of the tetraspanin super family and β1 integrin and regulates proliferation and migration of oligodendrocytes. *J. Cell Biol.* **153**, 295-306.

Todres, E., Nardi, J. B. and Robertson, H. M. (2000). The tetraspanin superfamily in insects. *Insect Mol. Biol.* **9**, 581-590.

Wu, V. M. and Beitel, G. J. (2004). A junctional problem of apical proportions: epithelial tube-size control by septate junctions in the *Drosophila* tracheal system. *Curr. Opin. Cell Biol.* **16**, 493-499.

Xu, H., Lee, S.-J., Suzuki, E., Dugan, K. D., Stoddard, A., Li, H.-S., Chodosh, L. A. and Montell, C. (2004). A lysosomal tetraspanin associated with retinal degeneration identified via a genome-wide screen. *EMBO J.* **23**, 811-822.

Yanagihashi, Y., Usui, T., Izumi, Y., Yonemura, S., Sumida, M., Tsukita, S., Uemura, T. and Furuse, M. (2012). Snakeskin, a membrane protein associated with smooth septate junctions, is required for intestinal barrier function in *Drosophila*. *J. Cell Sci.* **125**, 1980-1990.

Yanez-Mo, M., Barreiro, O., Gordon-Alonso, M., Sala-Valdes, M. and Sanchez-Madrid, F. (2009). Tetraspanin-enriched microdomains: a functional unit in cell plasma membranes. *Trends Cell. Biol.* **19**, 434-446.

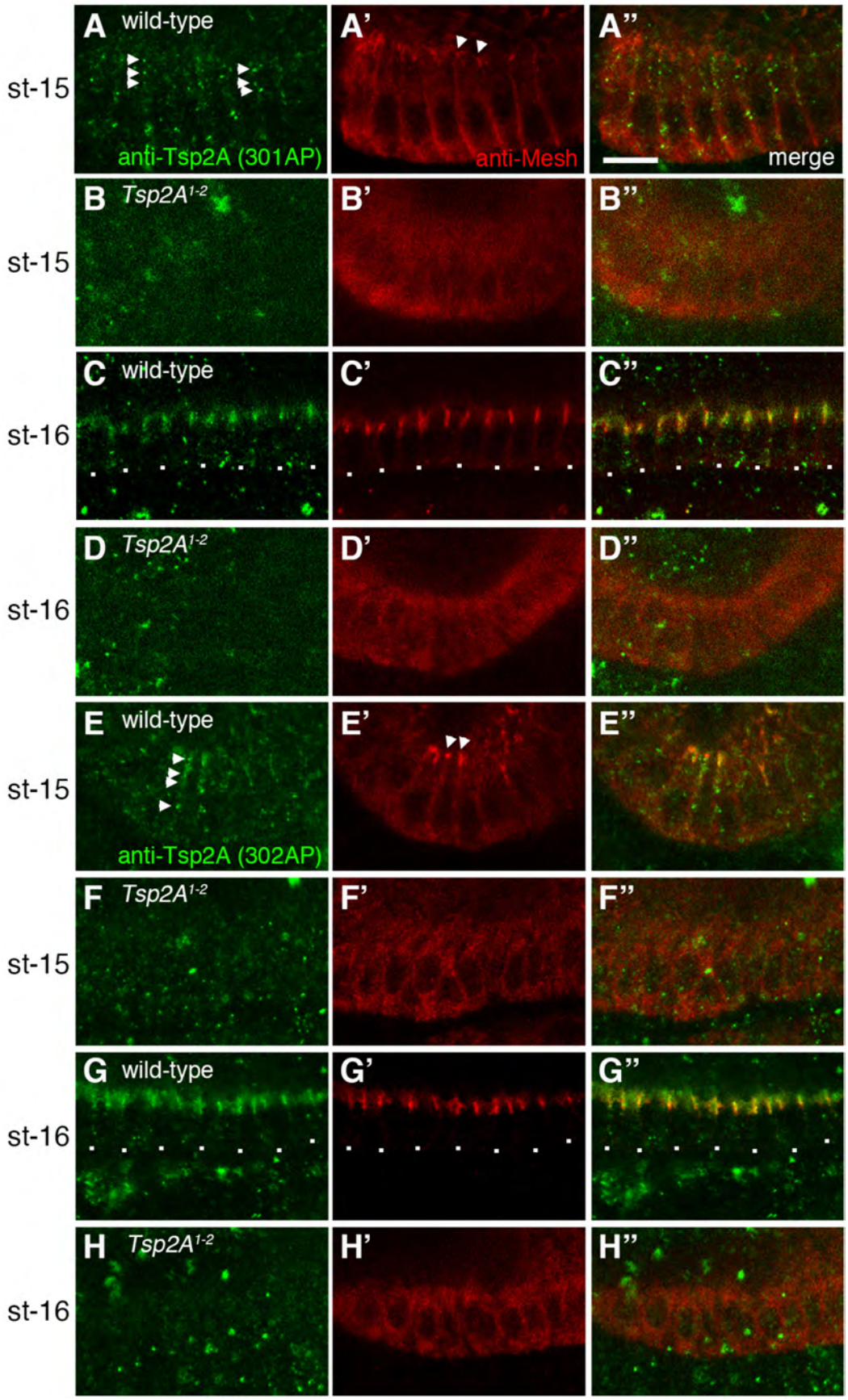

Figure S1. Tsp2A and Mesh distribution during sSJ formation in wild-type and *Tsp2A*$^{1-2}$-mutant embryos

(**A-H**”) Double-staining of stage-15 wild-type embryos (A-A” and E-E”), *Tsp2A*$^{1-2}$-mutant embryos (B-B” and F-F”), stage-16 wild-type embryos (C-C” and G-G”) and *Tsp2A*$^{1-2}$-mutant embryos (D-D” and H-H”) with a combination of anti-Tsp2A antibody (301AP for A-D or 302AP for E-H) and anti-Mesh antibody (A’-H’). Arrowheads in A and E indicate the aggregates of Tsp2A along the lateral membrane. Arrowheads in A’ and E’ indicate the apicolateral accumulation of Mesh. Scale bar: 5 μm (A-H”).

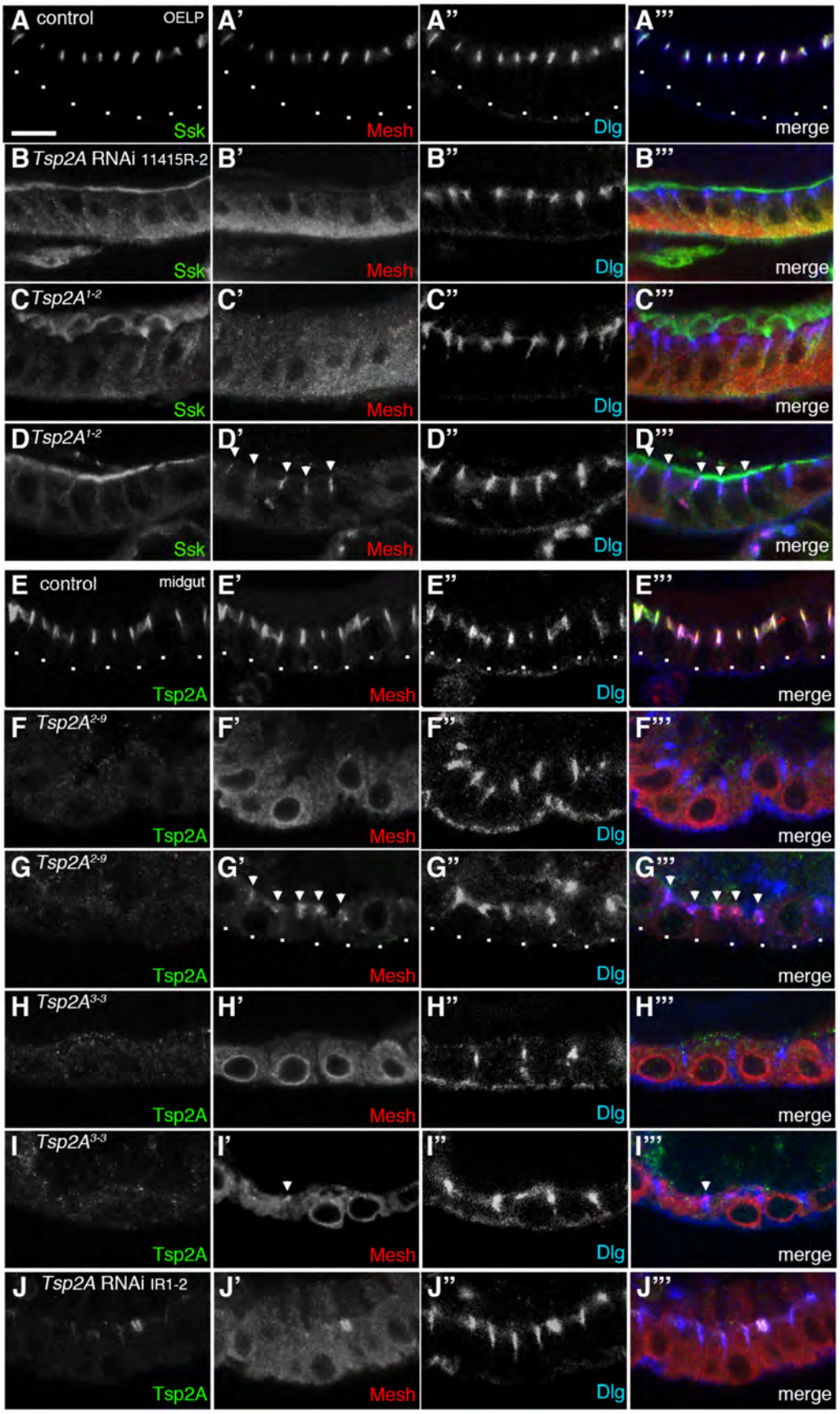

Journal of Cell Science • Supplementary information

Figure S2. sSJ components are mislocalized in *Tsp2A*-mutant epithelial cells.
(**A-D”’**) The first-instar larval OELP of control (A-A”’), *Tsp2A*-RNAi 11415R-2 (B-B”’) and $Tsp2A^{1-2}$-mutant (C-C”’ and D-D”’) stained with anti-Ssk (A-D), anti-Mesh (A’-D’) and anti-Dlg (A”-D”) antibodies. The merged images are shown in A”’-D”’, where the staining of anti-Ssk, anti-Mesh, and anti-Dlg is shown by green, red and blue, respectively. Arrowheads in D’ and D”’ indicate the apicolateral localization of Mesh in $Tsp2A^{1-2}$-mutant OELP.
(**E-J”’**) The first-instar larval midgut of control (E-E”’), $Tsp2A^{2-9}$ (F-F”’ and G-G”’), $Tsp2A^{3-3}$ (H-H”’ and I-I”’) mutants and *Tsp2A*-RNAi IR1-2 (J-J”’) stained with anti-Tsp2A (E-I), anti-Mesh (E’-I’) and anti-Dlg (E”-I”) antibodies. The merged images are shown in E”’-J”’. Arrowheads in G’, G”’, I’ and I”’ indicate the apicolateral localization of Mesh in $Tsp2A^{1-2}$-mutant epithelial cells. Basal membranes are delineated by dots. Scale bar: 5 µm.

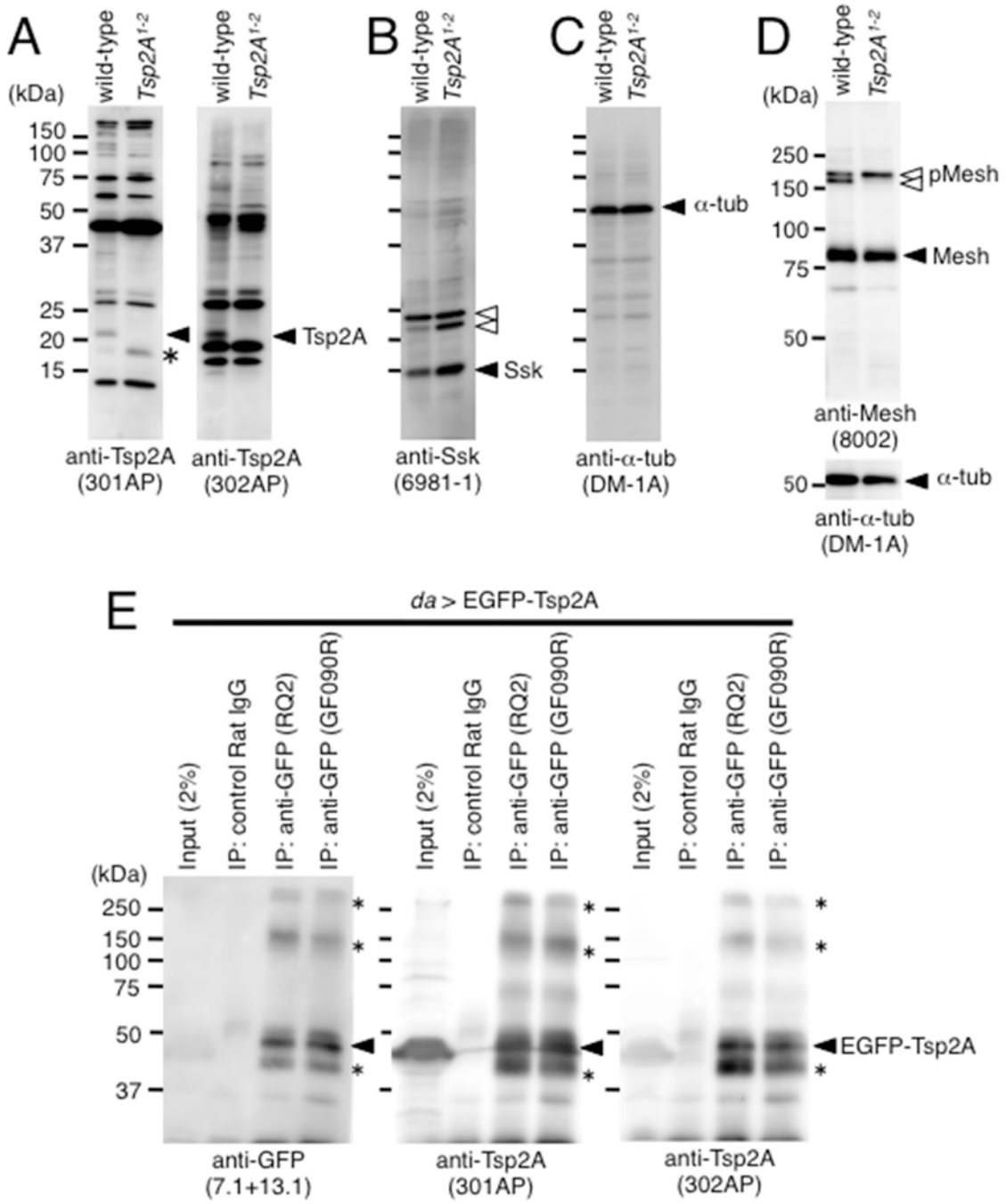

Figure S3. Anti-Tsp2A antibodies recognize endogenous and exogenous Tsp2A in Western blots.

(**A-C**) Extracts of the first-instar larva prepared from wild-type *Drosophila* and *Tsp2A*$^{1-2}$-mutants were separated on a 15% SDS-polyacrylamide gel, and Western blot analyses were performed using anti-Tsp2A (A, left panel, 301AP; right panel, 302AP), anti-Ssk (B) and anti-α-tubulin (C) antibodies. A protein band of ~21 kDa was detected by anti-Tsp2A antibodies in the wild-type but not in the *Tsp2A*$^{1-2}$-mutant (A; arrowheads), suggesting that the ~21 kDa band represents Tsp2A. Instead, an ~18 kDa band was detected by anti-Tsp2A antibody (301) in the *Tsp2A*$^{1-2}$-mutant extract (A; asterisk of left panel). Protein bands other than the ~21 kDa band, detected by each

anti-Tsp2A antibody seem to originate from cross-reactions because they are observed in both of wild-type and *Tsp2A*$^{1\text{-}2}$-mutant larvae (A). The density of the main band of Ssk (~15 kDa) is not significantly different in the *Tsp2A*$^{1\text{-}2}$-mutant relative to the wild-type (B; arrowhead). White arrowheads in B indicate non-specific bands detected by anti-Ssk antibody. Western blots using anti-α-tubulin antibody show that the same quantities of protein were loaded in the wild-type and *Tsp2A*$^{1\text{-}2}$-mutant extracts (C).

(D) Extracts of first-instar larvae prepared from wild-type *Drosophila* and the *Tsp2A*$^{1\text{-}2}$-mutant were separated on an 8% SDS-polyacrylamide gel and Western blot analyses were performed using anti-Mesh (D; upper panel), and anti-α-tubulin (D; lower panel) antibodies. The density of the main band of Mesh is not significantly different in the *Tsp2A*$^{1\text{-}2}$-mutant compared with the wild-type (D; arrowhead). However, the higher-molecular-mass band of Mesh is visible as a double band at ~200 kDa in the wild-type (upper and lower white arrowhead) but as a single band in the *Tsp2A*$^{1\text{-}2}$-mutant (upper white arrowhead). Western blots using anti-α-tubulin antibody show that the same quantities of protein were loaded in the wild-type and *Tsp2A*$^{1\text{-}2}$-mutant extracts (lower panel).

(**E**) The extracts of embryos expressing EGFP-Tsp2A with the *da*-GAL4 driver (Input) were subjected to immunoprecipitation (IP) with rat IgG and two kinds of anti-GFP antibodies (RQ2 or GF090R). The immunocomplexes were separated on a 12% SDS-polyacrylamide gel and Western blot analyses were performed using anti-GFP antibody (left panel) or anti-Tsp2A antibody (301AP; middle panel or 302AP; right panel). In addition to the main band of EGFP-Tsp2A (arrowhead), weak bands at 250, 150, and 40 kDa are detected by these antibodies (asterisks). In the input lanes, the specific bands of EGFP-Tsp2A were undetectable by these antibodies.

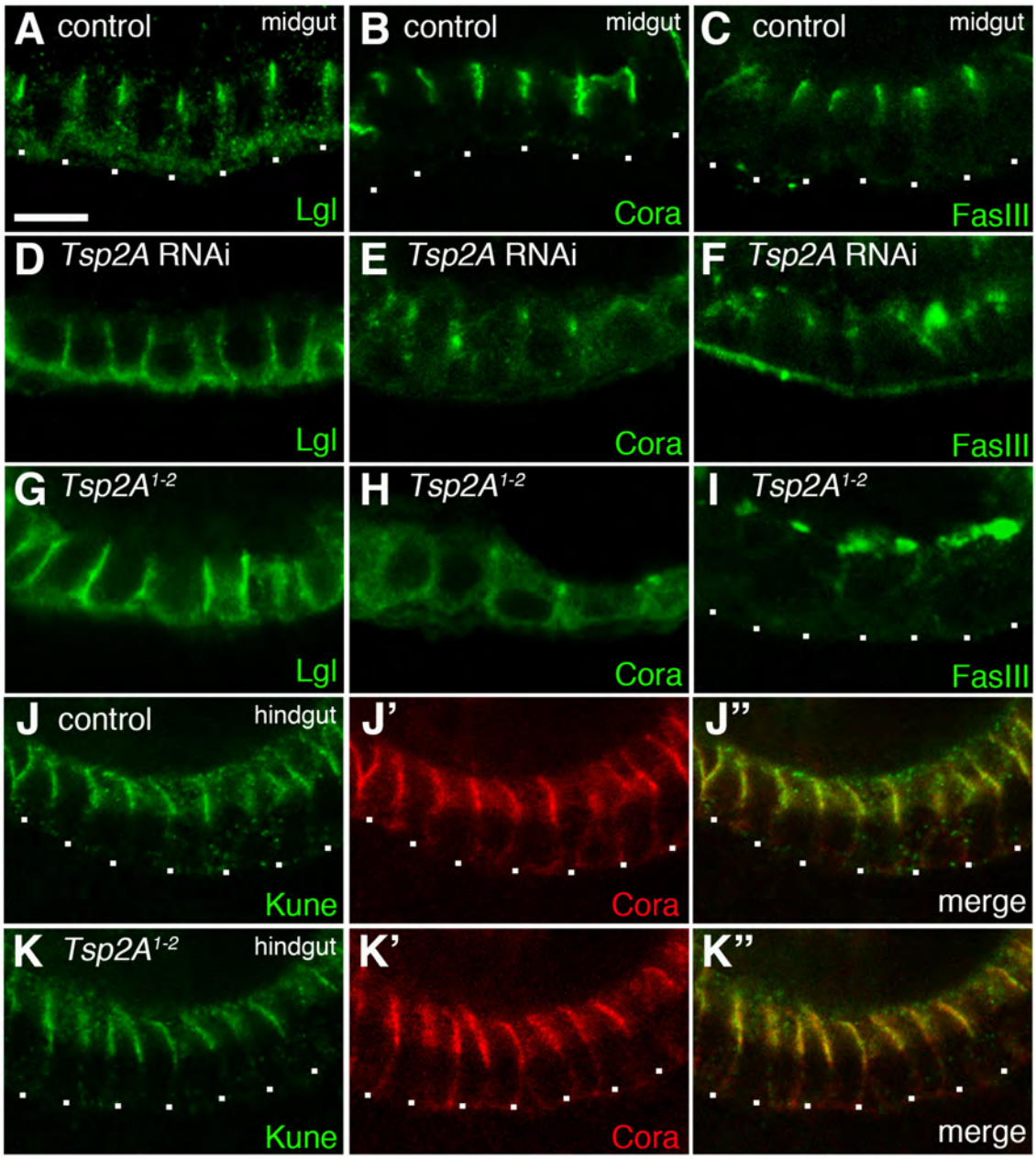

Figure S4. A *Tsp2A* mutation causes mislocalization of SJ components in the midgut.

(**A-I**) The first-instar larval OELP of control (A-C), *Tsp2A*-RNAi 11415R-2 (D-F) and $Tsp2A^{1-2}$-mutant (G-I) stained with anti-Lgl (A, D and G), anti-Cora (B, E and H) and anti-FasIII (C, F and I) antibodies.

(**J-K"**) Antibody double-staining of stage-16 control (J-J") and $Tsp2A^{1-2}$-mutant (K-K") embryos using anti-Kune (J and K) and anti-Cora (J' and K') antibodies. The merged images are shown in J" and K". Basal membranes are delineated by dots. Scale bar: 5 µm.